International Journal of Computer Information Systems and Industrial Management Applications
ISSN 2150-7988 Volume 18(21s) 2026 pp. 1559-1580
https://doi.org/10.70917/ijcisim-2026-5876
Article

Enhancing 5G Base Station Placement in Outdoor 3D Environments Using a Quantum Genetic Algorithm

Meenaz Shaikh[1], Ashwani Kumar Yadav2, Siraj Pathan[3]

[1]Department of Electronics & Communication Engineering, Amity School of Engineering and Technology, Amity University Rajasthan, India, Email ID:- meenazshaikh88@gmail.com
[2]Electronics & Communication Engineering, Amity School of Engineering & Technology, Amity University Rajasthan, India Email ID:- akyadav@jpr.amity.edu
[3]Reliance Jio Mumbai, India. Email ID:- siraj.pathan@ril.com

Abstract: The proliferation of fifth-generation (5G) base stations has introduced significant challenges related to suboptimal deployment and escalating construction expenses. To address these issues, this paper introduces an optimization methodology for 5G base station placement, specifically applied to a district in Kowloon, Hong Kong, which balances the competing objectives of signal coverage and deployment cost through a weighted approach. Our approach begins by simulating signal propagation using detailed three- dimensional (3D) maps combined with ray-tracing models. We incorporate demographic data to generate a realistic, random distribution of users along the map's street-level areas. We identify viable candidate sites for new base stations, considering both ground-level and rooftop installations, while imposing constraints on the tower heights. To mitigate construction expenditures, the model also evaluates the integration of pre-existing base station infrastructure. Furthermore, a novel dynamically adjusted quantum genetic algorithm (DAQGA) is proposed to determine the optimal base station configuration, using network coverage and construction cost as its primary objective functions. The efficacy of the resulting layout is assessed using a metric based on signal reception strength. The simulation results confirm that this optimization technique successfully pinpoints coverage blind spots in the planning zone, highlighting connectivity failures attributable to building-induced signal obstruction or locations outside the service range. An optimal trade-off between deployment objectives is achieved when the weights for coverage and cost are assigned values of 0.7 and 0.3, respectively. When benchmarked against four alternative algorithms, our proposed improved algorithm demonstrates superior performance in both convergence rate and solution stability.
Keywords: Base station deployment; Fifth generation (5G); Path loss; Ray tracing model; Three-dimensional map (3D); Quantum genetic algorithm (QGA)

1. Introduction

Global communication technologies are advancing at an unprecedented pace, establishing fifth-generation (5G) networks as a foundational pillar of the modern information society. This 5G-driven landscape has seen an explosive increase in the user base, consequently placing more stringent demands on the infrastructure, particularly base station deployment. Base stations function as the critical nodes for wireless connectivity. A lack of scientific foresight in their planning and placement can result in significant resource wastage and signal interference. Such issues directly degrade network coverage, signal quality, and the end-user experience, while simultaneously complicating network management and elevating operational expenditures. Moreover, suboptimal base station layouts may create bottlenecks that restrict future technological upgrades and development pathways, potentially impeding the forthcoming evolution toward 6G networks [6]. It is, therefore, imperative to research and implement effective deployment strategies. This is critical not only for improving the quality of current network services but also for ensuring sufficient capacity for the growth of future communication technologies.

Copyright: © 2026 by the authors

Historically, optimizing 5G base station placement has depended on three main pillars: manual human expertise, specialized simulation software, and algorithmic optimization [1],[3]. The manual-expertise approach is generally confined to the initial planning phases. It involves planners using factors like user density, existing 4G infrastructure, and communication data to select 5G site locations. This method, however, is heavily reliant on subjective judgment and individual experience, a dependency that can introduce decision inconsistencies and reduce placement accuracy. It also lacks the agility to adapt quickly to environmental shifts or urgent network demands. Furthermore, as networks scale to include hundreds or thousands of nodes, a deployment strategy centered on human expertise becomes entirely impractical.

To surmount these limitations, the industry frequently employs wireless network simulation software like Mapinfo and Atoll. These tools significantly lessen the manual workload and can forecast the performance of different deployment layouts. A drawback, however, is their typical reliance on empirical path loss models, such as the

Okumura-Hata, COST231-Hata, and other standard propagation models. Such models must be calibrated with real-world path loss data and their accuracy is tightly coupled to specific propagation environments [9],[10]. The rapid evolution of urban landscapes means that new environments require fresh on-site measurements, which restricts the general applicability of these calibrated models. Compounding these issues are the high licensing costs for such simulation tools and their frequent inability to integrate critical factors, like construction costs, into their layout predictions.

In the quest for more efficient and cost-effective solutions, intelligent optimization algorithms have seen widespread application in addressing base station coverage problems.

These algorithms operate by iteratively evaluating solutions against multiple constraints to identify an optimal deployment layout. This automated approach improves network performance and resource utilization, reduces manual labor and time investments, and adeptly balances the trade-off between network coverage and construction costs[12],[13].

A significant limitation of existing research, however, is its predominant reliance on two-dimensional (2D) mapping for placement optimization [7],[19]. This 2D focus commonly neglects two critical factors: the signal-shielding effects of buildings and the profound impact that antenna height has on both the coverage footprint and signal quality. Furthermore, many studies do not account for non-uniform user density in different areas or the potential performance implications of deploying diverse types of base stations.

2. Related Work

A substantial body of previous research has investigated base station deployment strategies powered by intelligent optimization algorithms. This work has leveraged advanced algorithms—including the sparrow algorithm, artificial immune system algorithms, and genetic algorithms—in an effort to discover optimal layouts within complex network topographies.

For instance, Chang et al. [16] discretized the target coverage area into pixels to maximize the covered region using an improved sparrow search algorithm. Focusing on green networking, Wang et al. [17] introduced a deployment method for micro base stations in ultra-dense heterogeneous networks, balancing energy efficiency and electromagnetic radiation against user quality-of-service standards. Similarly, Seda et al. [18] focused on optimizing the number of 5G service centers required to meet specific user demands. Wang et al. [19] combined Geographic Information Systems (GIS) with heuristic algorithms to spatially simulate 5G signal propagation and optimize

service coverage. Gou et al. [20] put forward an efficient strategy for micro base station deployment by simultaneously optimizing their quantity, location, and power, thereby enhancing adaptability to varied user distribution patterns. In another study, Dong et al. [21] formulated a constrained minimum-cost framework for millimeter-wave BS deployment in Manhattan-like grid environments, seeking the best balance between station density and transmission power.

Despite these advances, a common shortcoming persists: most research centered on intelligent algorithms operates within 2D map environments. This approach fundamentally neglects the influence of real 3D geography on signal propagation and fails to model the realistic, street-level distribution of users.

The combination of exponential user growth and the persistent challenge of achieving deep 5G coverage has prompted researchers to investigate hybrid deployments of macro and micro base stations, optimized via intelligent algorithms. Wang et al. [22], for example, proposed one such hybrid method that considered both cost and coverage. A significant limitation of their work, however, was the reliance on idealized circular coverage models, which failed to capture the nuances of real-world scenarios or specific coverage radii parameters. In a different approach, Chen et al. [23] applied the k-means clustering algorithm to analyze weak-signal data. They then formulated a single-objective nonlinear programming model aimed at minimizing the construction cost of new stations, subject to constraints on inter-station distance and minimum traffic coverage. A key oversight in this methodology was its failure to assess whether the identified centers of weak-coverage zones were actually viable locations for construction.

Concurrently, a distinct research vein has emerged focusing on the use of unmanned aerial vehicles (UAVs) as mobile, flying base stations to extend cellular coverage, often optimized within 3D maps. Sobouti et al. [26] proposed a solution for joint 3D localization and trajectory planning that incorporates altitude to minimize the user-to-UAV distance, using a Fuzzy Candidate Point Selection method to find optimal UAV locations. Parvaresh et al. [27] employed an Actor-Critic Deep Q-Learning algorithm for 3D UAV-BS deployment, with the goal of maximizing total network throughput. Lee et al. [28] developed a multi-agent Q- learning strategy for UAV deployment and power control, optimizing for energy efficiency and minimal user outages.

Rahimi et al. [29] investigated the localization and resource allocation for 3D UAV-based small cells, and in a separate work [30], they explored 3D localization to determine the minimum number of UAVs needed to cover IoT network users. Tarekegn et al. [31] proposed a hierarchical Deep Reinforcement Learning (DRL) approach that integrates link quality prediction with deep Q-learning for 3D drone mobility, showing superior performance in dynamic environments.

3. Motivation and Contribution

Motivated by the aforementioned shortcomings in 5G base station deployment, this paper introduces a 3D optimization scheme. Our method is tailored for deploying 5G base stations operating at 3.5 GHz in outdoor urban environments, with a specific focus on optimizing for variable antenna heights.

The primary contributions of this work are summarized as follows:

We utilize actual population density data to generate a realistic, random user distribution at street level within the 3D map. This distribution is intentionally weighted, with higher user concentrations in specific high-traffic scenarios, including commercial areas, parks, and schools.

We implement a multi-stage screening process for candidate base station locations to filter out unsuitable sites, such as roads, playgrounds, the rooftops of exceptionally tall buildings, and their immediate vicinities[19],[22]. For sensitive areas like schools, ground-level placements are excluded, though rooftop options are permitted. Crucially, distinct height restrictions are established for both ground and rooftop tower installations.

We frame the optimization problem from the operator's primary perspective, balancing network coverage against construction costs [14],[22]. Our method constructs optimal layouts for a variable number of base stations and provides a detailed analysis of the resulting signal reception strength distribution throughout the planning area.

We introduce a dynamically adjustable quantum genetic algorithm (DAQGA) to solve the optimal deployment layout [2],[7]. This algorithm features several enhancements: a microhabitat population initialization strategy based on a normal distribution; an optimized selection strategy for quantum gate angles, which dynamically adjusts rotation

angles based on fitness values in each iteration; and the integration of an elite individual preservation strategy alongside a catastrophe mechanism to avoid premature convergence to local optima.

Structure of this Article

The remainder of this paper is structured as follows: Section 2 details the environmental modeling, including the ray- tracing model used for path loss calculation in the 3D map and the methodology for random user distribution. Section 3 presents the DAQGA-based optimization strategy for base station deployment. In Section 4, we present and analyze the experimental simulation results. Finally, Section 5 provides the concluding remarks.

3. Signal Propagation Model an Environment Construction

This section describes the integration of ray-tracing models, 3D maps, and accurate, randomized personnel distributions. This combination is essential for the subsequent high- fidelity simulation of signal propagation, which in turn allows for precise evaluation of base station coverage and cost.

Ray Tracing Model

Ray tracing models are primarily based on the image method or the Shooting and Bouncing Rays (SBR) method [32]. SBR is capable of handling more complex environments and multiple reflection effects, yielding more accurate results than the image method. Furthermore, the computational complexity of SBR increases linearly with the reflection count, whereas the image method's complexity grows exponentially. For these reasons, this paper adopts SBR as the primary ray-tracing methodology.

Surface Material Effect

When radio waves interact with surfaces, the material properties of those surfaces influence the reflection loss. Ray-tracing models capture this propagation loss by considering the complex relative permittivity of a surface, which is a function of the material's relative permittivity and its conductivity.

The 3.5 GHz frequency band is particularly well-suited for high-capacity service in densely populated urban hotspots. While it may have more limited coverage distance and higher penetration loss compared to lower frequencies, its

selection is strategically sound[3]. The 3.5 GHz industry chain is mature, and its equipment supports dual-mode NSA/SA architecture, facilitating co-deployment with existing 4G networks and a smooth upgrade path to 5G Advanced, aligning with operators' phased upgrade strategies [6]. Furthermore, major markets like China and the EU have designated 3.5 GHz as a primary commercial 5G band, meaning that frequency division and interference management standards are well-established, reducing deployment risk.

Consequently, this study focuses exclusively on antennas operating at 3.5 GHz. The simulation models electromagnetic wave propagation interacting with building materials (concrete, glass, brick) and concrete terrain surfaces. Table 1 lists the specific parameters used for these materials.

Table 1: Materials parameters.

Material Class	Real Part of Relative Permittivity	Conductivity (S/m)
concrete	5.31	0.0899
glass	6.27	0.0192
brick	3.75	0.038

To balance computational efficiency with coverage accuracy in this large-scale scenario, we optimized the ray-tracing parameters. Referencing settings from [33] (4 reflections, 2 diffractions), preliminary simulations in MATLAB showed that calculating coverage for a single base station serving 5 users required 2 minutes. Reducing the diffraction

count to 0 drastically cut the computation time for a single base station covering all users to just 15 minutes. This change resulted in a negligible average received signal power difference of only 0.22 dB (sampled over 100 users). Therefore, we set the number of diffractions to 0 for this study. To compensate for potential propagation path loss from disabling diffraction, we increased the maximum reflection count to 10. The angular separation was set to a medium level, striking an optimal balance by avoiding the computational overhead of high-precision mode while preventing coverage gaps common in low-precision mode.

Reflection Loss

Reflection loss is computed by integrating Fresnel reflection coefficients, using Jones polarization vectors Jtx and Jrx to define the normalized electric field polarization at the transmitter and receiver, as shown in (1) [39]:

$$PL_{refl} = -20\log 10\left|J'_{rx} \times R \times J_{tx}\right|$$

Gas and Rain Propagation Model

The deployment method proposed here dynamically optimizes the layout based on annual environmental characteristics [3], [6]. By analyzing cyclical environmental changes, we formulate a sustainable plan that ensures the base station configuration maintains long-term regional adaptability. Incorporating the International Telecommunication Union's (ITU) models for gas and rain propagation into the ray-tracing framework significantly improves the prediction accuracy.

Gas loss, primarily caused by signal interaction with atmospheric oxygen and water vapor molecules, is given by (2)[36]:

$$PL_{gas} = (\gamma_o + \gamma_w) \times d$$

Where γo and γw represent the specific attenuation from dry air and water vapor, respectively. An annual average temperature of 27 degrees Celsius is assumed [36].

Rain-induced attenuation occurs as raindrops absorb and scatter radio wave energy[37]. This model helps predict system performance under adverse weather, as shown in (3):

$$PL_{rain} = m \times v^{\beta} \times d$$

Here, m and β are polarization coefficients. v is the rainfall intensity. Based on an average annual rainfall of 2400 mm, v is approximately 0.3mm/h, which corresponds to light rain [37].

D Map Construction and User Distribution

In 5G scenarios, signal propagation is highly susceptible to the 3D spatial structure. This section, therefore, uses 3D maps composed of various building materials and populates the streets with randomly distributed users to more accurately evaluate network coverage in complex urban environments.

Survey Region

We selected a 450,000 square meter area in Kowloon, Hong Kong, using publicly available data from Open Street Map. The region's latitude spans 22.3171942711 to 22.3226149837, and its longitude ranges from 114.174273101 to 114.181556891. The average building height in this area is 38 meters. Fig. 1 shows the 3D

map, where gray, blue, and red buildings are made of concrete, glass, and brick, respectively[19]. The terrain material is uniformly set to concrete to account for ground reflections



Fig. 1. Urban a 3D Layout of the area.

Distribution of User Candidate Positions

We used the 2020 spatial population distribution dataset for Hong Kong from NASA's Socio-Economic Data and Applications Center (SEDAC). This dataset, based on the WGS-84 coordinate system, records average 24-hour population density in a 1KM x 1KM grid . The region's population is estimated at 6,000. To achieve more accurate outdoor coverage simulation, we assume 55% of the population (3,300 users) is outdoors. Of these, 2,000 are randomly distributed across the entire region. To model varying densities, we added 700 people in school areas, 300 in park areas, and 300 around commercial buildings.

To simulate realistic activity patterns (e.g., on streets and in parks) and avoid placing users in non-conventional areas like rooftops, we defined exclusion zones through the following steps :

Building contour extraction and discretization: Building contour vector data was extracted via ArcGIS and discretized into a set of points at 1- meter intervals, from which geographic coordinates were extracted[19].

Terrain and surface feature integration: We integrated Digital Elevation Model (DEM) and Digital Surface Model (DSM) data to get the elevation for each discrete point. A "forbidden zone" rule was defined: if the DEM/DSM elevation difference at a building contour point exceeded 3 meters, all points within that building's area were marked as forbidden .

User location generation and avoidance: Using Matlab, initial user coordinates were randomly generated. The Haversine formula was used to check the distance to all forbidden points; if any user was within 1 meter of a forbidden point, the position was deemed invalid and regenerated .

Special Area Adaptation: For clearly labeled public areas (schools, parks) from Open Street Map, polygonal boundaries were extracted, and Matlab was used to generate uniform random points within them. For undefined areas (e.g.,

around commercial complexes), the adjacent street network was extracted via ArcGIS to construct closed polygons for random point generation. All generated points were cross- checked against the exclusion zones.

This process yields the realistic user distribution shown in Fig. 2, ensuring all users are on streets and not in unrealistic locations like rooftops. This approach better captures the impact of building obstructions on signal reception, helps identify coverage blind spots, and enables the design of more effective deployment strategies

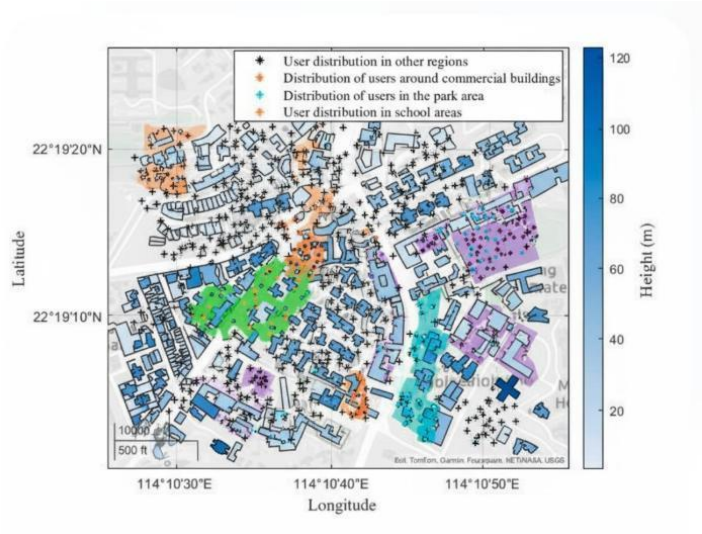


Fig. 2. User distribution.

2 Base Station Deployment Optimization Method Based on Dynamic Adjustment Quantum Genetic Algorithm

In this section, we present the two objective functions (cost and coverage) and the constraints governing the deployment parameters We also detail the improvements made to the traditional quantum genetic algorithm to better suit this optimization problem .

Optimize the Construction of Objective Function

We introduce the cost and coverage objective functions, detailing the factors for construction cost and the method for estimating coverage based on the population served .

Cost Objective Function

For ground-based stations, tower height dictates the required foundation depth. Using cost data from tower manufacturers, we generated a cost-fit curve for ground tower height (Fig.

3) [14]. The resulting quadratic fitting formula serves as the

cost function for ground towers, shown in (4) :

$$C_{suf} = a \times h_{suf}^2 + b \times h_{suf} + c$$
$$15 \leq h_{suf} \leq 40$$

where hsuf is the ground-based tower height (constrained between 15 and 40 meters), and a,b, and c are the linear relationship coefficients.

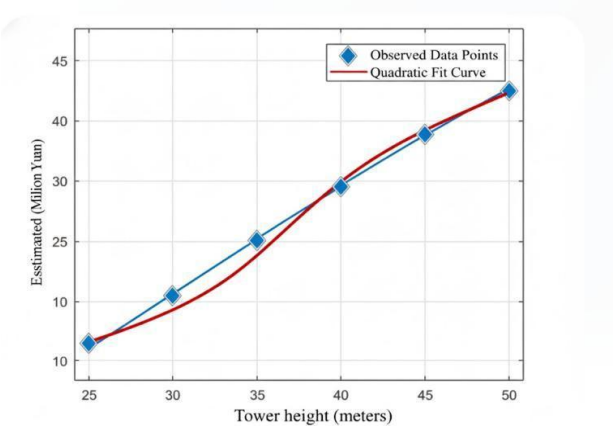


Fig. 3. Ground Base Station Cost Vs Tower Height. For rooftop-based stations, foundations are typically not

feasible. Thus, the tower cost is influenced only by its height, h_{top}. The cost formula is linear, as shown in (5):

$$C_{top} = p \times h_{top}$$
$$3 \leq h_{top} \leq 21$$

where p is the unit cost, and htop is constrained to between 3 and 21 meters based on practical considerations.

The cost for new base stations includes equipment and facilities, as represented in (6):

$$C_{new} = (p_{sn} + H_{sn}) \times N_{sn} + (p_{to} + H_{to})$$

(Note: Psn are power facility costs, Hsn are equipment room costs for new ground Nsn and rooftop Nto stations. M is the unit cost of communication equipment.

To save on investment, this study also considers utilizing existing base station infrastructure. In this case, tower costs are ignored, and costs are focused solely on equipment

expansion or upgrades, detailed in (7) :

$$C_{old} = (p_o + m) \times N_o$$

where Po and M are the unit prices for expanding power and communication equipment, respectively, and No is the number of existing stations utilized.

The overall cost function C is the sum of these components, shown in (8):

$$C = \sum_{1}^{N_{sn}} C_{suf} + \sum_{1}^{N_{to}} C_{top} + C_{new} + C_{old}$$

Covering Objective Function

The ray-tracing model calculates the path loss from a base station to every user. A user receives signals via multiple paths; if all path loss values are null, the user is in an area not covered by the signal. The total path loss PL is calculated as (9):

$$PL = PL_{refl} + PL_{gas} + PL_{rain}\sqrt{b^2 - 4ac}$$

Where PLrefl, PLgas, PLrain are the reflection, gas, and rain losses, respectively.

Due to obstructions, base station coverage is often not a perfect circle, so simple area ratios are inaccurate estimators. This study instead calculates coverage F by determining the fraction of the 3,300 randomly distributed users who can establish a connection, as shown in (10):

$$F = \frac{N_{peo} - N_{PL}}{N_{peo}}$$

Where Npeo is 3300, and Npl is the number of users not covered.

The cost and coverage functions operate on different scales, necessitating normalization of the cost function, as shown in (11):

$$C_{one} = \frac{C - C_{low}}{C_{high} - C_{low}}$$

Where Clow and Chigh are the minimum and maximum costs observed during optimization. The coverage value is already between 0 and 1 and requires no normalization.

The overall optimization function is illustrated in (12)

$$\begin{cases} Y = \lambda_1 \times F + \lambda_2 \times (1 - C_{one}) \\ \lambda_1 + \lambda_2 = 1 \end{cases}$$

Constraint Condition

To ensure the deployment parameters reflect real-world conditions, we introduce constraints on candidate locations, tower heights, and inter-station distances.

Base Station Candidate Location Constraints

Base stations are classified as new or existing. A grid of new candidate locations was set every 10 meters. To identify suitable construction sites, we implemented the following filtering steps:

Calculated the DSM/DEM height difference to exclude sites on rooftops of buildings taller than 35 meters.

Used ArcGIS to calculate building contours and exclude locations within 10 meters of them.

Obtained road network data to exclude sites within 10 meters of a main road center and 5 meters of a side road center.

Identified school zones via ArcGIS; since stations in these areas are typically on rooftops, ground candidate sites were excluded by comparing DSM/DEM heights.

Identified parks and playgrounds via ArcGIS and excluded candidate sites within them

These steps effectively filter unsuitable locations, significantly reducing the optimization time. An initial set of 10,000 new candidate sites was reduced to 551 effective candidate locations, which also included four existing base stations. The distribution of these locations is shown in Fig. 4.

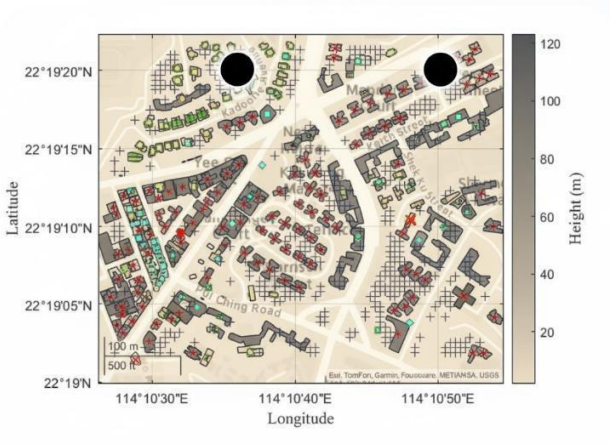


Fig. 4. Base station Sites.

In Fig. 4, the **crosshatch patterns** represent viable filtered sites suitable for new ground stations. The **teal-colored building rooftops** are identified as centroids where new rooftop stations can be constructed. **Red 'X' icons** indicate rooftops that are unsuitable for new construction. The **large black circles** denote existing base stations, with their coordinates sourced from OpenCellID. For data reliability, only stations established within the last three years were considered. The key parameters for this existing base station dataset are detailed in Table 2.

Table 2: Existing base station parameters.

Radio	Mcc	Area	Lon	Lat	Created	Updated
LTE	454	2110	114.17865	22.31866	2023/7/21	2023/7/21
LTE	454	2102	114.181106	22.319731	2023/7/21	2023/7/21
LTE	454	31	114.180617	22.322065	2023/7/21	2023/12/11
LTE	454	66	114.174451	22.320216	2023/11/23	2023/11/23

New Ground Base Station Tower Height Constraint

Based on planning reports and manufacturer data, urban ground towers (like single-tube or landscape towers) generally range from 30 to 45 meters. We set the maximum ground tower height hsuf to 40 meters. The minimum height must be sufficient to clear surrounding low- to mid-rise buildings, so it is set to the average height hmean of these buildings. This average hmean ranges from 9 to 40 meters in the study area.

$$h_{mean} \leq h_{suf} \leq 40$$

New Rooftop Base Station Tower Height Constraint

For rooftop stations, the antenna height is the sum of the building height hbuild and the rooftop tower height htop. Rooftop towers are generally not built very high (max 21 meters from manufacturers) due to material and wind pressure constraints. The total antenna height is also capped at 40 meters.

We established constraints to ensure the minimum antenna height exceeds the average building height hmean. A boundary condition occurs at a building height of 19 meters, as a 21-meter tower on such a building reaches the 40-meter total antenna height limit.

When the average building height hmean exceeds 19 meters,

the conditions in Fig. 5 apply:

$$h_{mean} - h_{build} \leq h_{top} \leq 21$$
$$h_{mean} - h_{build} \leq h_{top} \leq 40 - h_{build} \quad 19 \cdot$$
$$3 \leq h_{top} \leq 40 - h_{build} \qquad h_{mea}$$

When hmean does not exceed 19 meters, the conditions in Fig. 6 apply:

$$h_{mean} - h_{build} \leq h_{top} \leq 21 \qquad h_{build} \leq$$
$$3 \leq h_{top} \leq 21 \qquad h_{mean} < h_{bu}$$
$$3 \leq h_{top} \leq 40 - h_{build} \qquad 19 < h_{build}$$

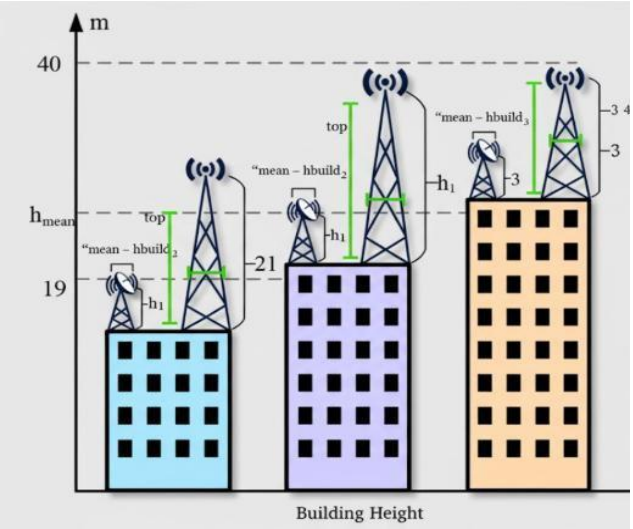


Fig. 5. Diagram of an average height exceeding 19 meters.

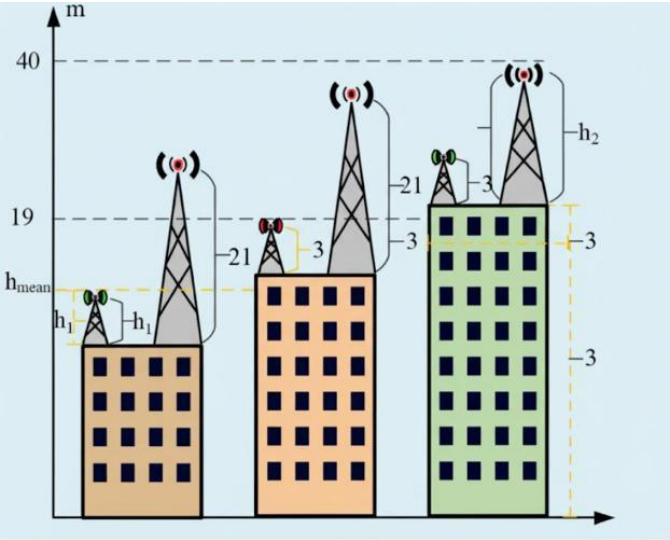


Fig. 6. Diagram of an average height not exceeding 19 meters.

Interference Constraints Between Base Stations

To prevent excessive coverage overlap in dense urban areas, we impose a minimum distance constraint dlimit between any two base stations I and j. Distances dij are calculated using the Vincenty formula.

$$d_{ij} \leq d_{limit}$$
$$d_{limit} = 1.5 \times R$$

Where R is the base station coverage radius.

DAQGA Algorithm Implementation

To make the algorithm better suited for the base station deployment problem, we introduce improvements in three areas: population initialization, the quantum rotation gate, and a quantum catastrophe mechanism.

Microhabitat Population Initialization Based on Normal Distribution

The conventional Quantum Genetic Algorithm (QGA) typically initializes all quantum bits with identical probability amplitudes. This uniform distribution can result in candidate solutions that are too evenly spread, failing to adequately explore the most promising regions of the solution space. This limitation is particularly detrimental when tackling complex, multi-peak optimization problems

To find the optimal base station strategy, this paper integrates QGA with a microhabitat population technique [7]. This hybrid approach achieves two goals: it broadens the algorithm's search range and ensures the initial population is dispersed across the solution space, which facilitates multi- directional searching. A key benefit of this is the prevention of premature convergence to a local optimum.

Each individual q is defined by a set of base station parameters (location and height). This individual is then quantum-encoded. The population is divided into n subpopulations (microhabitats) to balance global and local search. Within the jth subpopulation, the kth quantum bit [ak, Bk]T for all individuals is initialized with the same probability amplitudes:

$$q = \left[g_1, g_2, \cdots, g_{e/2}, g_{e/2+1}, \cdots, g_e\right]$$

Where, g1, g2, ⋯, ge/2 is the set of base station positions, ge/2+1, ⋯, ge is the set of base station heights, and e is the

number of base stations

$$Q_j = \left[q_{j,1}, q_{j,2}, \cdots, q_{j,i}, \cdots, q_{j,l}\right]$$
$$q_{j,i} = \left[g_1^{j,i}, \cdots, g_{e/2}^{j,i}, g_{e/2+1}^{j,i}, \cdots, g_e^{j,i}\right] = \left[\begin{array}{c|c|c|c|c} \alpha_1 & \alpha_2 & \cdots & \alpha_k & \cdots & \alpha_m \\ \beta_1 & \beta_2 & \cdots & \beta_k & \cdots & \beta_m \end{array}\right]$$
$$\begin{bmatrix} \alpha_k \\ \beta_k \end{bmatrix} = \begin{bmatrix} \sqrt{\frac{j}{n}} \\ \sqrt{1-\frac{j}{n}} \end{bmatrix}$$

This defines the chromosome Qj for the jth subpopulation. Each quantum exists in a superposition of states

While a uniform superposition ak = Bk is good for the initial global search, the quantum revolving door will gradually guide the population toward the current optimum. If the search space has multiple local optima, this can lead to premature convergence.

To resolve this, we propose a microhabitat strategy where the size of each subpopulation is governed by a normal distribution **(shown in figure x).** This introduces a natural, non-uniform distribution among the population groups. This method maintains population diversity while simultaneously concentrating search efforts on regions of the solution space that are potentially more advantageous, balancing global and local search. This approach

significantly improves convergence speed compared to a purely global search. The continuous normal distribution function is discretized for this application.

$$f(x|\mu,\sigma^2)$$

Figure x

Dynamic Selection Strategy for Quantum Rotation Gate

In QGA, updates to the base station parameters (position and height) are achieved by applying a quantum rotation gate Utheta to the quantum bits:

$$U(\theta)=\begin{bmatrix}\cos\theta & -\sin\theta\\ \sin\theta & \cos\theta\end{bmatrix}$$

This updates the probability amplitudes. The algorithm's convergence speed is highly dependent on the rotation angle theta. A fixed angle cannot dynamically balance the needs of the search: early-stage global exploration requires a large angle, while late-stage local exploitation requires small- angle fine-tuning.

We, therefore, improve the rotation angle adjustment strategy. The angle theta is dynamically adjusted based on the difference between the optimal fitness fitbest and the current individual's fitness fit, using (12) as the fitness function. A larger fitness difference necessitates a larger rotation, and a smaller difference requires a smaller, fine-tuning rotation. The strategy is given by:

$$\theta = k \times \pi \times (1 + (fit_{best} - fit)/fit_{best}/2)$$

where k is a coefficient (default 0.01), fitbest is the optimal fitness, and fit is the current individual's fitness.

Quantum Cataclysm Adjustment Strategy

If the optimal solution's fitness stagnates over several consecutive iterations, it strongly suggests the algorithm is trapped in a local optimum. Standard QGAs lack a built-in "catastrophe" mechanism to escape this stagnation.

Our strategy involves a catastrophe event: we preserve the top 25% (approximately) of the current optimal deployment parameters, plus the best-known historical parameter. This elite preservation prevents the loss of good solutions. The remaining 75% of the population is then completely reinitialized using the normal-distribution-based microhabitat strategy. This process allows the algorithm to rapidly escape the local search and resume its pursuit of the global optimum.

Simulation

Simulation experiments were conducted using MATLAB 2023b on a Windows 10 system with an Intel Core i7-8700

CPU and 16GB of memory. The key system parameters are listed in Table 3.

Table 3: System parameter setting

Parameter	Numerical Value
survey algebra	450000 m²
evaluation algebra	400
population size	40

number of new base station locations	547
number of existing base station locations	4
total population	3300
user device height	1.5 m
the power allocated by the base station to each user	30 dBm
antenna frequency	3.5 GHz
type of transmitting/receiving antenna	Omnidirectional antenna

An ablation analysis (Table 4) was performed to determine the optimal population size and iteration count, testing combinations of population sizes (30, 40, 50) and iterations

(300, 400, 500). The results in Table 4 indicate that a

population size of 30 yielded consistently lower mean objective function values. Conversely, population sizes of 40 and 50 produced comparable mean objective function values and tended to terminate around 200 generations. To balance the need for clear convergence observation with computational load, we selected a population size of 40 and a maximum iteration count of 400 for all subsequent experiments.

coverage increases and the weighting for cost decreases, the network's coverage capability improves, which corresponds to an increase in construction cost. The layout strategy also shifts, prioritizing new ground stations more heavily as coverage becomes more important

Table 4: Parameter test results.

Number of populations	number of iterations	Mean of objective function	Average number of termination iterations
30	300	0.6743	274.3
30	400	0.6316	280.65
30	500	0.6595	285.15
40	300	0.7645	219.95
40	400	0.7791	232.9
40	500	0.7411	223.35
50	300	0.7703	193.85
50	400	0.7658	191.2
50	500	0.7493	189.35

For presentation, candidate sites are numbered: 1-316 (new ground), 317-318 (existing ground), 319-320 (existing

rooftop), and 321-551 (new rooftop). In this complex 3D

environment, 2-8 stations are typically required for coverage. A market fluctuation coefficient (S) is included in

cost calculations.

The results of varying the coverage (m1) and cost (m2) weights are presented in Table 5. As the weighting for

Table 5: Base station deployment results

	m1 m2	Coverage rate	Cost	Base station location	Tower height	Antenna height	Number of base stations
1	0.9 0.1	87.45%	247.80 x	323 193 548	8 37 8 14	39 37 23 38 40 40	6/0
			S	353 413 499	19 16		
2	0.8 0.2	86.55%	207.31 x	319 500 261	8 14 28 5	32 38 28 34 33 23	5/1
			S	341 402 546	11 14		
3	0.7 0.3	85.42%	146.75 x	530 317 320	21 38 8 5 6	38 33 38 30 35 39	4/2
			S	423 343 405	15		
4	0.6 0.4	80.93%	143.25 x	319 318 333	11 37 9 5	35 37 33 27 21 36	4/2
			S	402 536 341	12 7		
5	0.5 0.5	75.75%	107.25 x S	320 319 423 500 437	8 8 3 3 11	33 32 36 27 20	3/2

The data indicates that the optimal balance between coverage and cost is achieved when the weights are set to 0.7 for coverage and 0.3 for cost (Option 3). This third scenario represents an ideal balance. It deploys six stations (four new rooftop, one existing ground, one existing rooftop) for a cost of $146.75 \times S$ and achieves 85.42% coverage.

While this configuration results in a minor coverage reduction (2.32% and 1.31%) compared to the first two, more coverage-focused options, it achieves substantial cost savings of 40.78% and 29.21%, respectively. In contrast, the fourth and fifth options, which prioritize cost, suffer from significantly poorer coverage (5.55% and 12.77% less than option 3). The first option (0.9/0.1 weights) achieved maximum coverage (87.45%) by using all-new stations, but at the highest cost (247.80 x S). The fifth option (0.5/0.5 weights) had a low cost but a significantly deficient coverage of 75.75%. We, therefore, conclude that the third option (0.7/0.3) is the superior solution for the deployment problem investigated in this study.

Fig. 7 plots the fitness value against the number of base stations, confirming that the objective function peaks when six base stations are deployed. When the number increases to seven or eight, the fitness value plummets because the interference constraints (minimum distance) cannot be met

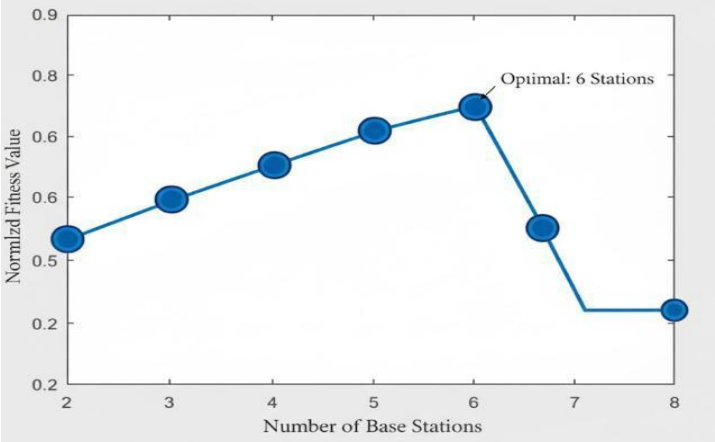


Fig. 7. The variation of fitness value with the number of base stations.

The optimal coverage map for this 6-station layout is shown in Fig. 8. Red icons mark the final base station locations. Signal strength attenuates with distance , and the minimum inter-station distance was set at 250 meters to prevent interference. The simulation effectively identifies real-world coverage failures; for instance, "Uncovered user 1" (Fig. 9) is blocked by a building obstruction , whereas "Uncovered user 2" (Fig. 9) is simply outside the service range. The base station coverage optimization method successfully mirrors real-world scenarios and visually exposes signal blind spots.



Fig. 8. The optimized Network Coverage.

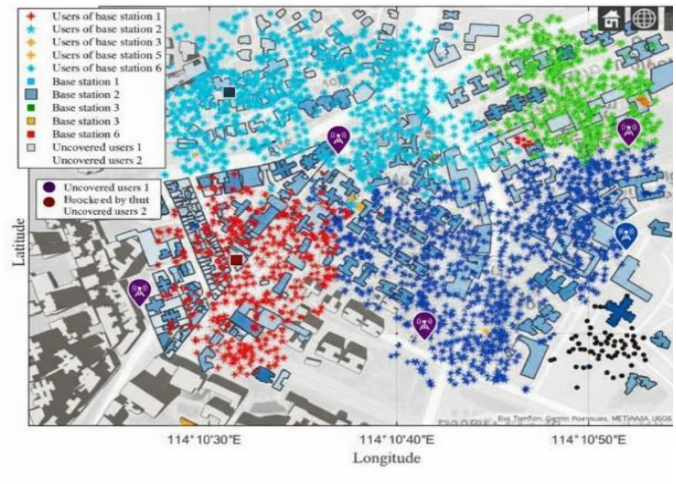
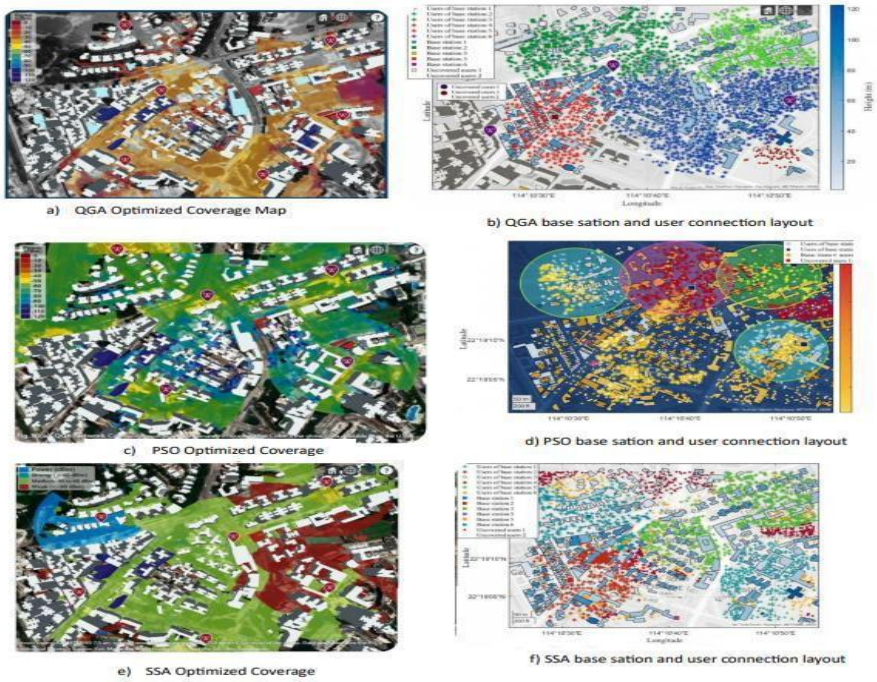
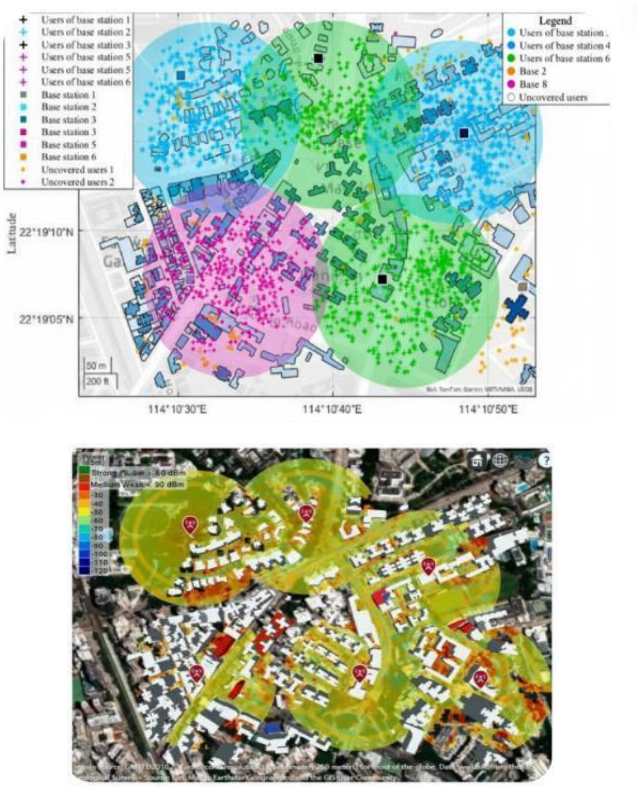


Fig. 9. Connection diagram between base station and users.

advantages were observed against SSA (10.5% better coverage, 18.02% lower cost) and AMGA (5.82% better coverage, 28.51% lower cost).





(g) AMGA optimized coverage

Fig. 10. Deployment optimization diagram

Table 6: Comparison of optimization results of different algorithms.

	Coverage rate	Cost	Base station location	Tower height	Antenna height	Number of base stations
QGA	75.21%	168.19 x S	320 317 458 44 383 483	8 37 11 21 11 4	33 37 20 21 22 28	4/2
PSO	72.24%	244.74 x S	365 456 208 95 317 227	13 11 20 20 23 20	38 20 20 20 23 20	5/1
SSA	77.3%	179 x S	476 499 353 323 317 388	21 16 14 8 21 9	30 40 38 39 21 37	5/1
AMGA	80.72%	205.26 x S	252 464 341 499 547 319	26 11 5 16 13 10	26 20 34 40 28 34	5/1

DAQGA	85.42%	146.75 x S	530 317 320 423 343 405	21 38 8 5 6 15	39 38 33 38 30 35	4/2

The coverage maps in Fig. 10 visually confirm this quantitative data; the four competing algorithms fail to provide uniform coverage, leaving significant blind spots in both dense building clusters and open-area roads. In contrast, the DAQGA-optimized layout (Fig. 8) is more evenly distributed and minimizes large blind spots, clearly outperforming the alternatives.

The convergence curves in Fig. 11 further highlight DAQGA's superior performance. While SSA and AMGA converge quickly (before 150 generations), they fall into local optima early. QGA suffers from instability and late convergence (around 350 generations). PSO shows a very slow convergence trend. In contrast, DAQGA exhibits robust, step-wise growth before entering a stable convergence phase around the 220th generation , achieving the best overall balance between stability and final fitnes. Statistical analysis (Table 7) using the Wilcoxon rank-sum test (p=0.05) confirms that DAQGA is statistically superior to all comparative algorithms.

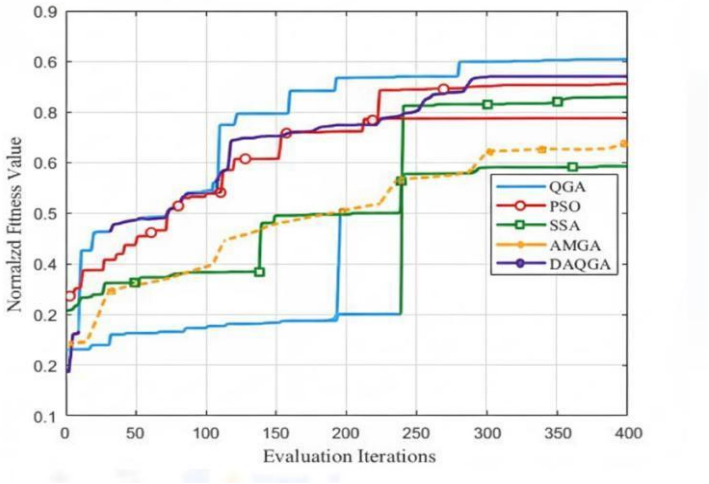


Fig. 11. Convergence curves of various algorithms

Table 7: Comparison table of algorithm performance.

DAQG A	AMGA	QGA	SSA	PSO
0.7997	0.7314	0.7135	0.6551	0.7291
(0.0088)	(0.0315)	(0.0804)	(0.0715)	(0.0744)
	-	-	-	-

Finally, Fig. 12 illustrates the signal reception strength distribution, a fundamental metric for coverage quality. We set a communication threshold of -95 dBm. The DAQGA- optimized layout achieved an effective average signal strength of -69.74 dBm, with 75.03% of user locations exceeding the -95 dBm threshold. This is a marked improvement over the other algorithms: QGA (-97.25 dBm; 68.06%), PSO (-103.27 dBm; 64.18%), SSA (-108.14 dBm;

65.54%), and AMGA (-72.73 dBm; 70.63%). Our DAQGA

algorithm improved the effective average signal reception strength by 27.51 dB (vs. QGA) to 38.4 dB (vs. SSA) and increased the probability of a quality connection by 6.23% (vs. AMGA) to 16.91% (vs. PSO). This confirms the DAQGA approach significantly enhances both cost- efficiency and communication quality.

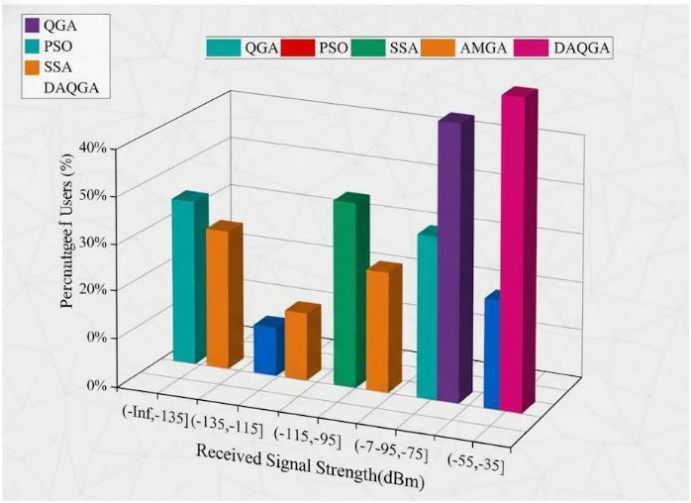


Fig. 12. Signal reception intensity ratio diagram at different stages.

4. Conclusion

This paper presented an in-depth investigation into the critical factors governing 5G base station deployment—including type, location, and height—and proposed a novel DAQGA algorithm to find the optimal layout. Our methodology began by spatially distributing users at street level in a 3D map, using a ray-tracing model for accurate signal simulation. Next, we applied a series of realistic siting constraints to filter candidate locations. Finally, we employed the DAQGA to solve the dual-objective optimization problem, balancing coverage and cost to identify the best configuration.

The planning scenario selected for this research, composed mainly of dense areas with some sparse regions, is representative and lends a degree of generality to the findings. Consequently, the proposed method demonstrates good adaptability and can be extended to other environments by adjusting key parameters. For example, in ultra-dense urban or rural areas, interference distance constraints would need resetting. Similarly, if applying this method to millimeter-wave (mmWave) bands, which are highly sensitive to line-of-sight (LoS) conditions, propagation parameters like reflection count and angular separation would require careful reconfiguration.

The proposed DAQGA algorithm shows exceptional capability in solving the 5G deployment optimization problem. A limitation of the current work, however, is its formulation as a weighted single-objective problem, whereas practical deployment involves multiple, often competing, objectives. To overcome this, future work will aim to develop a true multi-objective optimization framework. This future framework will integrate other critical considerations, such as energy efficiency and the complexities of heterogeneous macro-micro station networks. Furthermore, we plan to incorporate additional key network parameters, including antenna azimuth and tilt angles, to enhance the model's realism and promote its application in next-generation wireless networks

REFERENCES

1. C.C. Kao, H.C. Young, Opportunities, challenges, and solutions in the 5G era, IEICE Trans. Commun. 105 (11) (2022) 1291–1298.
2. J.P. Li, J.J. Pang, X.J. Fan, Optimization of 5G base station coverage based on self-adaptive mutation genetic algorithm, Comput. Commun. 22 (2024) 83–95.
3. Y.C.O. Imam-Fulani, et al., 5G frequency standardization, technologies, channel models, and network deployment: advances, challenges, and future directions, Sustainability 15 (6) (Mar 2023) 1–71.
4. J.P. Li, P. Xue, T. Yang, W.T. Wang, Pilot contamination suppression method for massive MIMO system based on ant colony optimization, Wirel. Netw. 28 (5) (2022) 1879–1888.
5. J.P. Li, M.L. Li, T. Yang, P. Xue, Low-complexity
6. wiener filter channel estimation algorithm in massive MIMO-OFDM system, J. Jilin Univ. (Eng. Technol. Ed.) 52 (01) (2022) 211–218.

7. W. Chen, X. Lin, J. Lee, A. Toskala, S. Sun, C.F. Chiasserini, L. Liu, 5G-advanced toward 6G: past, present, and future, IEEE J. Sel. Areas Commun. 41 (6) (Jun 2023) 1592–1619.
8. J.P. Li, G.C. Li, S.C. Chu, M. Gao, J.S. Pan, Modified parallel tunicate swarm algorithm and application in 3D WSNs coverage optimization, J. Internet Technol 23 (2) (2022) 227–244.
9. R. Ratheesh, M.S. Nair, P. Vetrivelan, J. Rajeswari, Throughput and coverage based Base Station-Relay Station deployment for 5G cellular network, Concurr. Comput. Pract. Exp. (2024 Apr 2024) 14.
10. N. Cota, A. Serrador, P. Vieira, A.R. Beire, A. Rodrigues, On the use of Okumura-Hata propagation model
11. on railway communications, Wirel. Pers. Commun. 93 (3) (Apr 2017) 725–736.
12. A. Halifa, E. T. Tchao, and J. J. Kponyo, "Investigating the best radio propagation model for 4G WiMAX networks deployment in 2530MHz band in Sub- Saharan Africa," Arxiv, preprint Oct 25 2017.
13. Y.S. Zheng, R. Yan, Y. Liu, Correction of radio wave propagation prediction model based on improved seagull algorithm in tunnel environment, IEEE Access 9 (2021) 149569–149581.
14. C.W. Tsai, S.J. Liu, An effective hyper-dense deployment algorithm via search economics. J. Amb. Intell.
15. Humaniz. Comput. 11 (6) (Jun 2020) 2251–2262. 293
16. H. Ganame, Y.Z. Liu, H. Ghazzai, D. Kamissoko, 5G base station deployment perspectives in millimeter wave
17. frequencies using meta-heuristic algorithms, Electronics 8
18. (Nov 2019) 24.
19. L. Liang, C. Fu, Y. Gao, T. Su, F. Wan, X. Xiong, M. Pan, W. Guan, An optimal siting and economically optimal
20. connectivity strategy for urban green 5G BS based on distributed photovoltaic energy supply, Energy Convers. Manag. 301 (Feb 2024) 20.
21. B.A. Tesfaw, R.T. Juang, H.P. Lin, et al., Multi-agent
22. deep reinforcement learning based optimizing joint 3D trajectories and phase shifts in RIS-assisted UAV-enabled wireless communications, IEEE Open J. Veh. Technol. 5 (2024) 1712–1726.
23. Z.Z. Chang, Q.H. Gu, C.W. Lu, Y.H. Zhang, S.L.
24. Ruan, S. Jiang, 5G private network deployment optimization based on RWSSA in open-pit mine, IEEE Trans. Ind. Inform. 18 (8) (Aug 2022) 5466–5476.
25. Y.J. Wang, P. Sun, X.M. Shi, L. Zhang, Green deployment method of micro base station for ultra-dense
26. heterogeneous cellular networks based on constrained dolphin swarm algorithm, IEEE Access 8 (2020) 5349–
27. 5362.
28. P. Seda, M. Seda, J. Hosek, On mathematical modelling of automated coverage optimization in wireless 5G and beyond deployments, Appl. Sci.-Basel 10 (24) (Dec
29. 2020) 8853.
30. Q. Wang, X. Zhao, Z.T. Lv, X.Y. Ma, R.T. Zhang,
31. Y.F. Lin, Optimizing the ultra-dense 5G base stations in urban outdoor areas: coupling GIS and heuristic
32. optimization, Sustain. Cities Soc. 63 (Dec 2020) 14.
33. W. Guo, J. Koo, L.F. Siddiqui, N.M.F. Qureshi, D.R.
34. Shin, QoS-aware energy-efficient MicroBase station deployment for 5G-enabled HetNets, J. King Saud Univ.- Comput. Inf. Sci. 34 (10) (Nov 2022) 10487–10495.
35. M.M. Dong, T. Kim, J.J. Wu, E.W.M. Wong, Cost-
36. efficient millimeter wave base station deployment in Manhattan-type geometry, IEEE Access 7 (2019) 149959–
37. 149970.
38. C.H. Wang, C.J. Lee, X.J. Wu, A coverage-based location approach and performance evaluation for the deployment of 5G base stations, IEEE Access 8 (2020) 123320–123333.
39. J. Chen, J.J. Tian, S.H. Jiang, Y.S. Zhou, H. Li, J. Xu, The allocation of base stations with region clustering and single-objective nonlinear optimization. Mathematics 10 (13) (Jul 2022) 1–19.
40. M.J. Sobouti, A.H. Mohajerzadeh, H.Y. Adarbah, Z. Raitimi, H. Ahmadi, Utilizing UAVs in wireless networks:
41. advantages, challenges, objectives, and solution methods, J. Veh. 6 (4) (2024) 1769–1800.
42. G.B. Tarekegn, R.T. Juang, B.A. Tesfaw, et al., A centralized multi-agent DRL-based trajectory control strategy for unmanned aerial vehicle-enabled wireless communications, IEEE Open J. Veh. Technol. (2024).
43. M.J. Sobouti, et al., Efficient fuzzy-based 3-D flying base station positioning and trajectory for emergency management in 5G and beyond cellular networks, IEEE Syst. J. 18 (2) (2024) 814–825.
44. N. Parvaresh, B. Kantarci, A continuous actor-critic deep Q-learning-enabled deployment of UAV base stations; toward 6G small cells in the skies of smart cities, IEEE Open J. Commun. Soc. 4 (2023) 700–712.
45.] S. Lee, H. Yu, H. Lee, Multiagent Q-learning-based multi-UAV wireless networks for maximizing energy efficiency: deployment and power control strategy design, IEEE Internet Things J. 9 (9) (2021) 6434–6442.
46. Z. Rahimi, R. Ghanbari, A.H. Mohajerzadeh, H. Ahmadi, 3D UAV small cell base station positioning and
47. resource allocation in cellular network: a stochastic
48. optimization approach, IEEE Internet Things 11 (6) (2023)
49. 10951–10963.
50.] Z. Rahimi, M.J. Sobouti, R. Ghanbari, S.A. Hosseini Seno, A.H. Mohajerzadeh, H. Ahmadi, H. Yanikomeroglu, An efficient 3D positioning approach to minimize required UAVs for IoT network coverage, IEEE Internet Things 9 (1) (2021) 558–571.

51. G.B. Tarekegn, R.T. Juang, H.P. Lin, et al., Deep- reinforcement-learning-based drone base station deployment for wireless communication services, IEEE
52. Internet Things J. 9 (21) (2022) 21899–21915.
53. Z.Q. Yun, M.F. Iskander, Ray tracing for radio propagation modeling: principles and applications, IEEE Access 3 (2015) 1089–1100.
54. S.D. Li, Y.J. Liu, L. Yao, W. Cao, improved channel model and analysis of the effect of bodies in curved tunnel using ray tracing, IEEE Antennas. Wirel. Propag. Lett. 19 (7) (Jul 2020) 1162–1166.
55. International Telecommunications Union Radiocommunication Sector. Effects of building materials and structures on radiowave propagation above about 100MHz. recommendation P.2040. ITU-R, approved
56. August 23, 2023.
57. R.A. Chipman, W.S.T. Lam, G. Young, Polarized light
58. light), Crc Press, 2018.
59. International Telecommunications Union
60. Radiocommunication Sector. Attenuation by atmospheric gases and related effects P.676-12. ITU-R, approved August 14, 2019.
61. International Telecommunications Union
62. Radiocommunication Sector. Specific attenuation model for rain for use in prediction methods. Recommendation P.838-3. ITU-R, approved March 8, 2005.
63. J. Xue, B. Shen, A novel swarm intelligence
64. optimization approach: sparrow search algorithm, Syst. Sci. Control Eng. Open Access J. 8 (1) (2020) 22–34.
65. J.P. Li, J.J. Pang, X.J. Fan, Optimization of 5G base station coverage based on self-adaptive mutation genetic
66. algorithm, Comput. Commun. 225 (2024)